AIAA/CEAS 99-1924

Aeroperformance and Acoustics of the Nozzle with Permeable Shell

M. Gilinsky
Hampton University, Hampton, VA, USA
I.M. Blankson
NASA Glenn Research Center, OH, USA
V.M. Kouznetsov
and
S.A. Chernyshev
Central Aerohydrodynamics Institute
(TsAGI), Moscow, Russia

5th AIAA/CEAS Aeroacoustics Conference
10-12 May 1999
Bellevue (Greater Seattle), WA

Aeroperformance and Acoustics of the Nozzle with Permeable Shell

Mikhail Gilinsky[†]
Hampton University, Hampton, Virginia 23668
Isaiah M. Blankson[††]
NASA Glenn Research Center, Ohio, 44135
Vladimir M. Kouznetsov[*]
Central AeroHydrodynamics Institute (TsAGI), Moscow
and
Sergey A. Chernyshev[**]
Central AeroHydrodynamics Institute (TsAGI), Moscow

ABSTRACT

Several simple experimental acoustic tests of a spraying system were conducted at the NASA Langley Research Center. These tests have shown appreciable jet noise reduction when an additional cylindrical permeable shell was employed at the nozzle exit. Based on these results, additional acoustic tests were conducted in the anechoic chamber AK-2 at the Central Aerohydrodynamics Institute (TsAGI, Moscow) in Russia. These tests examined the influence of permeable shells on the noise from a supersonic jet exhausting from a round nozzle designed for exit Mach number, M_e=2.0, with conical and Screwdriver-shaped centerbodies. The results show significant acoustic benefits of permeable shell application especially for overexpanded jets by comparison with impermeable shell application. The noise reduction in the overal pressure level was obtained up to ~5-8%. Numerical simulations of a jet flow exhausting from a convergent-divergent nozzle designed for exit Mach number, M_e=2.0, with permeable and impermeable shells were conducted at the NASA LaRC and Hampton University. Two numerical codes were used. The first is the NASA LaRC CFL3D code for accurate calculation of jet mean flow parameters on the basis of a full Navier-Stokes solver (NSE). The second is the numerical code based on Tam's method for turbulent mixing noise (TMN) calculation. Numerical and experimental results are in good qualitative agreement.

I. INTRODUCTION

Permeable (perforated) nozzles and other permeable devices were studied many years ago for different applications, both experimentally and theoretically (see, for example, the papers presented at the IAS Meeting in Los Angeles, 1954, [1], or the Russian book by G.L. Grodzovsky, et al. [2]) . It is well known that compression or rarefaction waves in a supersonic flow slowly damp when these waves reflect from solid walls or from free boundaries (such as density discontinuities). Research results have shown that it is possible to change the supersonic flow structure and flow type by changing the reflection quality of the permeable (or porous) wall using an appropriate permeability coefficient. In some cases, a permeability coefficient can be chosen so that the boundary doesn't reflect incoming disturbances. In particular, using such a boundary, we can obtain the possibility of controlling the flow velocity (Mach number) along the axis of the supersonic divergent nozzle portion, of smoothing out any supersonic flow unevenness, of increasing the permissible size of models tested in aerodynamic wind tunnels, etc.

The use of permeable bodies is a second area of application of this research. Permeability decreases the drag coefficient of such bodies because compression waves are weakened by reflection from the bow portion of the bodies with appropriate weakening of the bow shock waves, detached or oblique. The simple theory for the solution of this problem was proposed by Dr. Kh.A. Rukhmatulin [3]. The porous and permeable body applications are well modeled by the theoretical approach, in particular, in boundary condition formulations and by com-

[†] Research Professor, Senior Member AIAA
[††] Senior Scientist/Technologist, AIAA Associate Fellow
[*] Professor, TsAGI Acoustic Division Chief
[**] Senior Research Associate, Ph.D.

parison to the body drag, flow smoothness around the body, reduction of noise generated by flow interaction with the surface. For example, substantial reduction of noise produced by a supersonic jet exhausting from a CD nozzle can be obtained by using a porous centerbody instead of a solid centerbody. This approach was proposed in the invention of Dr. L. Maestrello [4], and some experimental acoustic test results were presented in his paper [5].

A third research application connected with permeable surfaces is parachute theory and experiments (see [6-8]). In contrast to the previous cases, in the parachute theory, different approximations for boundary condition formulation use the presence of a substantial normal impulse component to the surface which is comparable with the transverse component.

The goal of the research presented is to obtain more uniform flow parameter distributions at the nozzle exit for reduction of jet noise and simultaneously to increase the nozzle thrust. The main mechanism of interaction of pressure waves with solid and permeable nozzle wall leads to interference of contrary signed waves (compression and rarefaction) from the solid wall and lip line portions. As a result, reflected shock waves interact with rarefaction waves and become weaker. Hence, the gas flow is more uniform. We have assumed that this effect will favour noise reduction generated by the exhaust jet. Application of permeable shells or main nozzles, in some cases, increases the nozzle thrust. The experimental and numerical simulation results obtained, in general, confirm this assumption.

II. EXPERIMENTAL APPROACH AND ACOUSTIC DATA

2.1 Experimental tests at the NASA LaRC.

Several simple experimental acoustic tests for a spraying system (Figure 1) were conducted at the NASA Langley Research Center. These tests have shown appreciable jet noise reduction when additional cylindrical permeable shells were attached at the nozzle exit. Four shells were tested, one impermeable and three permeable. All cylindrical shells had the same size with the internal diameter, d_i=1in, external, d_e=1.2in, and length,l=5in; the hole diameter was d_h=0.015in.

Two examples of the shells covering the cylindrical pipe of the spraying device are shown in Figures 1a,b. The shell's location changed during the tests. The main tests were conducted using the second shell modification shown in Figure 1b. The permeable shell has two sets of through holes: 8 holes were located uniformly in the azimuthal direction along the perimeters of 7 cross sections of the cylindrical shell, (i.e. the total hole number in each set is 7x8=56). The inclination angle of the hole to the cylinder axis α was the same for each set and different for different sets. The angle changed in the range: $\alpha = 30^o, 45^o, 60^o$, and 90^o to the nozzle inlet. At first, the impermeable shell was tested. In this case, jet noise increased by comparison with noise production without any shell. Usually, a high frequency tone occured during the test with the impermeable shell. Then the tests of the permeable shells were conducted and the shell location changed by moving it downstream along the cylindrical pipe of the spraying device. By this, the open hole number increased, which resulted in an increase in the mass flow rate through the hole set or increase of the permeability coefficient of the shell, ε. Here ε=nx8xS_o/S_c, where n is number of open hole lines (corresponding cross sections with the holes), S_o and S_c the areas of a round unit hole and of the total cylindrical surface of the shell respectively. For some coefficient values, the jet noise was reduced and the high frequency tone completely disappeared.

2.2 Acoustic Tests at the TsAGI, Moscow.

The reason for these tests was the desire for a more accurate examination of this phenomenon. A permeable cylindrical nozzle was made and acoustic tests were conducted in the anechoic chamber AK-2 at the Central Aerohydrodynamics Institute (TsAGI, Moscow) in Russia. These tests were a continuation and improvement of some previous acoustic tests using the same acoustic measurement apparatus and the same methods. The previous test results were presented at the 4th AIAA/CEAS Aeroacoustics Conference in Toulouse, France, 1998, [9]. We believe that it is expedient to repeat some details of the previous approach.

2.2.1 A Screwdriver centerbody (plug geometry A Screwdriver centerbody surface belongs to a family of shapes formed by rectilinear intervals joining corresponding points of two different closed curves in space. In this case, a circle as an initial curve and one or several crossing rectilinear intervals as an end curve are used. Usually, these intervals are symmetrically located relative to a body's axis of symmetry.

One of many possible modifications of such ring-shaped nozzles with the Screwdriver and axisymmetric centerbodies were made and tested. This design is shown in Figure 2 (on the right) and in the large view in Figure 6. The draft of the meridional plane cross section for this design with the axisymmetric (conical) centerbody is shown in Figure 4a with the main dimensions of this design.

The 4-petal Screwdriver centerbody (SdCB) shown in Figure 6a contains a cylindrical centerbody which downstream of the external nozzle exit transfers to a Screwdriver shaped portion. There are several geometric parameters which define the centerbody: number of petals, petal size and centerbody length. The axisymmetric centerbody with conical or optimal contour in a meridional plane can be taken as a baseline centerbody for comparison and for definition of Screwdriver centerbody efficiency. In Figure 6a, the 4-petal SdCB is based on the conical reference centerbody (CCB) shown in Figure 6b. This SdCB surface is formed as follows. The 45°-arc of the cylindrical portion and ending vertical interval are divided by I subintervals $[a_i, a_{i+1}...a_I]$ and $[b_i, b_{i+1}...b_I]$ respectively, where i=0,1,2,...I. Then, the corresponding points a_i and b_i are joined by rectilinear or curvilinear intervals and these intervals form the needed surface. The corresponding cross section areas of CCB and SdCB designs are equal. These sections are located at the same distance from the nozzle throat (or the nozzle exit).

The manufactured SdCB shown in Figure 6a has curvilinear Screwdriver-shaped surfaces. Namely, longitudinal rectilinear lines are replaced by curvilinear lines so that they are a smooth continuation of corresponding straight lines on a cylindrical portion having a horizontal tangent at the end of a centerbody. Thus, these curves should have points of inflection so that they may be given by two power functions with conjugation at these points of inflection. In the simplest case, these functions can be written as follows: Let an initial point a_i and ending point b_i have Cartesian coordinates $x_o^o = 0$, $y_o^o = r_o \cos(\phi_i)$, $z_o^o = r_o sin(\phi_i)$, where r_o is the cylindrical portion radius and ϕ_i is the polar coordinate of the initial point. For uniform splitting, $\phi = (i/I)\pi/4$, $z_e = z_e^o(1 - i/I)$. The curve joining these points can be described in Cartesian variables as:

$$z(\xi) = z_o - a_z\xi^{p_1}, \qquad y(\xi) = y_o + a_y\xi^{p_2} \quad if\ 0 \le \xi \le \xi_c \tag{1.1}$$

$$z(\xi) = z_e + b_z(1-\xi)^{q_1}, \ y(\xi) = b_y(1-\xi)^{q_2} \quad if\ \xi_c \le \xi \le 1 \tag{1.2}$$

where p_1, q_1, p_2, q_2 are fixed even powers, and ξ_c is a fixed conjunction coordinate of the two power functions which can be varied. The coefficients a_z, b_z, a_y, b_y are defined from the conjunction conditions: equality of the function and its first derivatives so that, for example, for $p_1 = p_2 = p$ and $q_1 = q_2 = q$ these coefficients are:

$$a_z = \frac{qf(\xi_c)}{\xi_c^{p-1}}, \quad b_z = -\frac{pf(\xi_c)}{(1-\xi_c)^{q-1}}$$

$$f(\xi_c) = \frac{(z_o - z_e)}{q\xi_c - p(1-\xi_c)}. \tag{1.3}$$

In accordance with formulae (1.1-1.3) with p=q=3.0 and characteristic lengths shown in Figure 4a, nozzles with SdCB and CCB were designed and drawn at NASA LaRC and then manufactured and tested at TsAGI, Moscow in Russia.

2.2.2 Supersonic CD Nozzle with Permeable and Impermeable Shells. The previous acoustic tests of the nozzles with the SdCB and CCB have shown an absence of any acoustic and aeroperformance benefits of a SdCB application by comparison with a CCB application. Moreover, for some angles $\theta = 90°$, a noise increase was observed $\sim$ 1-2%. The conclusion in the report [9] was to continue these tests by moving the centerbody into the nozzle and a using permeable nozzle wall. For some reasons, moving the centerbody upstream has been found more difficult than to use continuation of the external nozzle cylindrical portion (the shell). This shell is mounted on the external main nozzle so that the internal shell diameter is equal to the nozzle exit diameter and the shell ending axial coordinate, x_s, is equal to the ending centerbody axial coordinate, x_{cb}. The perforated shell has the hole row along the axis x containing 23 holes with 3mm diameter. Twenty-six such rows are located on the shell cylindrical surface almost uniformly in the azimuthal direction ϕ. Thus, the entire hole number is $23x26$=598 which corresponds to perforation (permeability) coefficient ~0.18. All other geometric parameters are shown in Figure 4b.

The nozzle pressure ratio (NPR) is varied in the interval π_c=2.5-4.5 with a cold, supersonic jet exhaust. For

the nozzle tested with centerbody shown in Figure 4a, the design Mach number at the original nozzle exit, i.e. at the entrance to the shell, x_e, equals $\sim M_e$=3.67, and nozzle pressure ratio, $NPR_e = p_t/p_e$=96.34. These values are based on a quasi-one-dimensional theory. Therefore, for the nozzle without any shell, the jets are essentially overexpanded in the entire interval of total pressure, and downstream from the exit intensive shock waves are formed. These shock waves reflect repeatedly from the centerbody and mixing layer (jet boundary). These shock waves are also formed when the solid shell is attached to the nozzle. The shock waves reflect from the two solid boundaries, centerbody and cylindrical wall of the shell. Note that a quasi-one-dimensional theory is not accurate enough for this case because of the shock waves presence.

2.2.3 Acoustic Data. The permeable shell can weaken shock waves and reduce broadband shock noise as well as turbulent mixing noise. For examination of this concept, several experimental and numerical tests were conducted. Acoustic tests were conducted in the anechoic chamber of the Central AeroHydrodynamics Institute (TsAGI, Moscow). The interior dimensions of the facility within the wedge tips are 9.6x5.3x4.2m high. Three nozzle designs with exhaust jets were tested. All designs had the axisymmetric external nozzle described above and two different internal parts: **a)** the coaxial 4-petal Screwdriver shaped centerbody (SdCB), **b)** the coaxial axisymmetric centerbody with the length and cross sections equal to the Screwdriver shaped centerbody (CCB). Three cases were tested: **1)** without any shell, **2)** with perforated shell, and **3)** with solid shell. All these designs were tested with the two nozzle pressure ratios: NPR=2.5 and 4.5. In addition, in the case **1b**, an additional test with NPR=3.5 was conducted. These cases are enumerated in Table 1 from 1 to 14 for more convenient acoustic results illustration.

The measurement procedure in the anechoic chamber and the method of automatic data processing are illustrated in Figure 5. Microphones (model 4136/Bruel& Kjaer Co) with cathode followers (model 4633) are positioned in the meridional plane on a circular arc with the radius R_m=2m with different observation angles θ to a positive (downstream) jet axis in the interval $30^o \leq \theta \leq 105^o$. Microphone signals are transmitted to the magnetic recorder "Sony KS-616U" through an amplifier (model 2608). Decoding of acoustic pressure pulsations was conducted by an analyzer (model 2032/Bruel&Kjaer Co.) and PC-286 computer which provided a narrow band spectrum with a band width $\sim \Delta f$=32Hz. A Pentium computer was used for transformation of narrow band spectra to 1/3-octave spectra.

Some experimental acoustic results are illustrated in Figures 7-9. In each graphic, two or three curves are presented. The curves differ by color and each of them are denoted by two numbers divided by a dash (or only two numbers for black curves). The first number designates the observation angle $\theta = 30^o, 45^o, 60^o$, or 90^o, and the second number designates the case number shown in Table 1. Blue lines denote the case without any shell, red lines are with perforated shell, and yellow lines are with solid shell.

Acoustic benefits of the perforated shell application take place for two observation angles 30^o and 45^o even by comparison with the cases of shell absence. It is remarkable because nozzle thrust in the first case is obviously more than in the latter cases by additional compression waves reflected from the shell wall. Numerical simulation results confirm this assertion (see below). More direct comparison of the two cases, with solid and perforated shells, is presented below. Figures 8 and 9 illustrate substantial acoustic benefits from perforated shell application in all observation angles. In Figure 8, the narrowband spectral density vs frequency is shown for both cases, and in Figure 9, 1/3-octave band spectral density vs frequency is shown for the same cases.

Note that in the best cases for the nozzle with conical centerbody (No. 1-3) and Screwdriver centerbody (No. 12-14), the overall acoustic pressure level for the nozzle with perforated shell is less than for the nozzle with the solid shell up to ~5-8%. For the highest nozzle pressure ratio, NPR=4.5, the combination of perforated shell and Screwdriver centerbody gives less acoustic benefits (No. 4-6).

III. NUMERICAL SIMULATION RESULTS

Numerical simulation of a jet flow exhausting from a convergent-divergent nozzle designed with $M_e = 2.0$ and with a permeable shell was conducted at the NASA LaRC and Hampton University. Two numerical codes were used. The first is the NASA LaRC CFL3D code [10] for accurate calculation of jet mean flow parameters on the basis of a full Navier-Stokes solver (NSE). The

second is the numerical code based on Tam's method [14,15] for turbulent mixing noise (TMN) calculation. Numerical and experimental results are in good agreement.

3.1 Mean Flow Numerical Simulation.

Aeroperformance effects and gas dynamic flow characteristics were analyzed numerically. The nozzle thrust calculations were based on a full Navier-Stokes equation solver (NSE), and both full and marching Euler codes: CFL3D [10], CRAFT [11], and Krayko-Godunov [12]. Grid preparation and optimization was conducted using GRIDGEN and our own codes. The main results were obtained using 2D and 3D versions of the CFL3D code which allows the simulation of both inviscid and viscous flows. This code is described in detail in the CFL3D User's Manual (Version 5.0) [10]. In accordance with this manual's introduction ([10], page 1): " ...CFL3D (Version 5.0) is a Reynolds-Averaged thin-layer Navier-Stokes flow solver for structured grids... CFL3D solves the time- dependent conservation law form of the Reynolds-averaged Navier-Stokes equations. The spatial discretization involves a semi-discrete finite-volume approach.

Upwind-biasing is used for the convective and pressure terms, while central differencing is used for the shear stress and heat transfer terms. Time advancement is implicit with the ability to solve steady or unsteady flows. Multigrid and mesh sequencing are available for convergence acceleration. Numerous turbulence models are provided, including 0-equation, 1-equation, and 2-equation models. Multi-block topologies are possible with the the use 1-1 blocking, patching, overlapping, and embedding. CFL3D does not contain any grid generation software. Grids must be supplied extraneously."

In the paper [9], the coordinate system, grid generation, necessary sizes of numerical domains, and minimal acceptable number of grid points and their distribution were described in detail. Note here that we were used the same as in [9] Menter's $k-\omega$ SST turbulence model [13]. We will omit other details (refer to the paper [9] (see p.6 and Figure 1)), and will consider only the boundary condition formulation at the permeable (perforated) shell wall. In general, that differences the presented research from the previous.

3.1.1 Boundary Condition Formulation for Permeable Walls.

It is well known that compression or rarefaction waves in a supersonic flow slowly damp when these waves reflect from solid walls or from free boundaries (such as density discontinuities). Research results [1,2] have shown that it is possible to change supersonic flow structure and flow type by changing the reflection quality of a permeable (or porous) wall using an appropriate permeability coefficient. In some cases, a permeability coefficient can be chosen so that the boundary doesn't reflect incoming disturbances. In particular, using such a boundary, we can obtain the possibility of controlling the flow velocity (Mach number) along the axis of the supersonic divergent nozzle portion, of smoothing out any supersonic flow unevenness, of increasing permissible sizes of tested models in aerodynamic wind tunnels, etc.

The flow at a perforated wall is complicated: through some holes, the gas injects into the main flow, and through others, a gas suction takes place. These processes become more complicated by viscous effects, in particular, by the friction at the solid wall portion. In many cases, the detailed flow at the each hole is not important, but merely the influence of their presence. The solution of the problem for supersonic flow at the permeable wall requires specific boundary conditions. Several approaches are used for such formulations. These are enumerated below with a short presentation of the final results:

a) The linearized theory. The assumptions are: 1. A small difference between pressures at the contrary sides of the wall (1 and 2), $\Delta p = p_2 - p_1 << p_i$ (i=1,2). 2. A hole size along the wall, X, much larger than the hole size in the normal direction to the wall, Y, i.e. the velocity component along the wall , u_i, is much bigger than that in the normal direction v_i. 3. The wall is plane. The permeable wall is considered as a surface with some alternative set of slots, i.e. solid and lip shock (density discontinuity) surfaces. Therefore a small perturbation theory leads to the simple formulae [2]:

$$\frac{v'}{u'} = \frac{S}{1-S}\sqrt{M_i^2 - 1} \quad if \quad M_i > 1 \qquad (3.1)$$

$$\frac{v'}{u'} = \tan\frac{(\pi}{2}S)\sqrt{1 - M_i^2} \quad if \quad M_i < 1 \qquad (3.2)$$

where the main flow at the wall with the corresponding Mach number M_i is directed along the wall, x, u', v' are velocity perturbations in the X and Y directions respectively, $S = S_h/(S_h + S_s)$ is a perforation coefficient, S_h is total hole area, and S_s is total solid wall area. These formulae provide the boundary conditions which allow calculation of the disturbed main flow on both sides of the wall. Note that in this approach, any mass flow rate through the holes is absent.

b) The Shock/Rarefaction Wave Method. In this approach, a 2D uniform supersonic flow of width H, with pressure, p_1, Mach number M_1 meets the permeable plane wall portion of length L at the angle, α. Then L=H/$sin\alpha$. The permeability is distributed uniformly along the wall. Dependent upon the pressure ratio at the permeable wall, $p_{21} = p_2/p_1$, a shock wave ($p_{21} > 1$) or centered (Prandtl-Meyer) rarefaction wave ($p_{21} < 1$) is formed. Thus, instead of at the angle α, the flow crosses the wall at some bigger angle $\theta = \alpha + \Delta\alpha$. The effective permeability coefficient S_* is defined as a ratio of linear portion of the wall which the flow crosses to the wall L_*=H/$sin\theta$, i.e. $S_* = L_*/L$. For pressure ratios, $p_2$1, close to 1, again simple formulae can be written.

For example, for a cross slot permeable wall:

$$\eta = \Delta p/\frac{\rho u^2}{2} = \frac{2(h/b-1)}{\alpha\sqrt{M_1^2-1}} \qquad (3.3)$$

where the effective permeability coefficient $S_* = b/h = \alpha/(\alpha+\Delta\alpha)$ is equal to the ratio between the slot width, b, and distance between neighboring slots, h.

c) The Mutually Penetrating Continua Theory. In accordance with this theory [3,6,8], the permeable surface is considered as a discontinuity over which the crossing gas flow loses some normal impulse component, R_n, s.t.:

$$[p + \rho u_n^2] = -R_n, \quad [\rho u_n u_\tau] = 0 \qquad (3.4)$$

$$[\rho u_n] = 0, \quad [\frac{(u_n^2+u_\tau^2)}{2} + \frac{\kappa}{\kappa+1}\frac{p}{\rho}] = 0 \qquad (3.5)$$

where u_n, U_τ are normal and transverse velocity components to the boundary, and κ is the specific heat ratio. An interphase reaction force R_n is defined from special experiments or from semiempiric theory. Using a quasi-one-dimensional theory inside a hole and the hydraulic approximation $-[p] = au_n + bu_n^2$, an approximate formula is presented in the paper [8] for the density ratio $\rho_{12} = \rho_1/\rho_2$:

$$\rho_{12} = 1 + \frac{\kappa}{2}\xi M_1^2 \sin^2\varphi + o(M_1^2\sin^2\varphi) \qquad (3.6)$$

where ξ is a hydraulic loss coefficient depending on the permeability coefficient S, local Reynolds number, Re, and hole shape. For example, for hole with sharp edges and large Reynolds numbers, the ξ is:

$$\xi = \frac{1}{S^2}(1 - S + 0.707\sqrt{1-S})^2$$

and for holes with smoothed edges:

$$\xi = k(1-S) + (1/S-1)^2, \quad k \sim 1$$

d) The Porosity Coefficient Definition. In the simplest semiempiric theory [1,6], the porosity coefficient R_p is directly introduced as a ratio between pressure gradient through the permeable wall, Δp and mass flow rate through the wall ρu_n, i.e.

$$R_p = \frac{\rho U_o u_n}{\Delta p} \qquad (3.7)$$

where U_o is the imperturbable mean flow velocity along the wall, and $K_p = R_p/U_o$ is assumed to be a constant along the wall. This is for walls made of so called linear porous material. For some walls and mean flow with direction close to normal to the wall, in accordance with [6] a quadratic relationship rather than linear is appropriate. The porosity coefficient usually is used as close to the permeability coefficient S which is defined above as a ratio between hole area and total wall area.

3.1.2 Numerical Simulation Results. With the purpose of understanding and optimization of the permeable design for acoustic benefits, several numerical simulations were conducted at the NASA LaRC and Hampton University. Unfortunately, at the present time we do not have the capability to calculate noise from a 3D jet exhausting from a Screwdriver nozzle. Hence, we conducted a numerical simulation for an axisymmetric CD round nozzle designed for exit Mach number, $M_e = 2.0$. The geometric parameters of this nozzle are close to the external nozzle tested at the TsAGI with axisymmetric and Screwdriver centerbodies. All the dimensions are shown in Figure 4a. The

reference Reynolds number is calculated on the basis of critical parameters at the nozzle throat and with the characteristic length equal the throat radius, $Re_* = \rho_* r_* c_* / \mu_* = 0.128 * 10^5$, where subscripts correspond to the parameters at the throat and μ is the dynamic viscosity coefficient. The cylinder shell (impermeable or permeable) is attached to the nozzle exit. The diameter of the shell is equal to the diameter D_e of the nozzle exit. The length of the shell is equal to D_e. A numerical simulation of the jet mean flow and sound radiated by the jet have been carried out in this work. The mean flow was evaluated on the basis of the NASA LaRC CFL3D code. The codes for sound radiation evaluation have been developed by the authors on the basis of Tam's method [14-15]. Three cases have been considered: Case I. Overexpanded jet (NPR=6.31). The cylinder shell is impermeable. Case II. Overexpanded jet (NPR=6.31). The cylinder shell is permeable (coefficient of permeability Kp=Cq/Δp=const, Cq is the mass flow rate through the cylinder wall per unit area, Δp is the difference between pressures on the outside and inside walls of the shell, and the value of the nondimensional coefficient of permeability is chosen to be equal 0.2). Case III. Underexpanded jet (NPR=9.47). The cylinder shell is permeable (Kp=0.2). Some of the results of mean flow evaluations are presented in Figure 10 (Mach contours) and Figure 11 (pressure contours). The mean flow evaluation allows us to draw the following conclusions:

1. The permeable cylinder shell can be used as a facility for smoothing of the supersonic jet exhausted at the off-design conditions (for both overexpanded jet and underexpanded jet). The intensity of barrel-shaped shock waves decreases substantially when a permeable cylinder shell is used. Barrel-shaped shock waves for case I are seen clearly (the upper picture in Figure 10) and these shock waves have almost disappeared for the cases II and III (the middle and lower pictures in Figure 10). The cause of the flow smoothness can be explained by the fact that pressure along the wall inside the permeable shell changes downstream of the nozzle exit to the value of the external pressure (in the ambient air). At the same time, for the impermeable shell the jet exhausted from the shell is essentially overexpanded. (Compare the cases II, III with the case I in Figure 10).

2. The velocity profile of the flow at the shell exit is not uniform. In case II, there is a flux of air into the shell through the permeable wall. This flux leads to slowing of the flow layers close to the wall. On the contrary, in the case III, there is an air flux directed out of the shell which causes acceleration of the flow layers close to the wall (Figure 11.)

These jet qualities are important for noise generation by the wave emission mechanism as well as by the broadband mechanism. In the next paragraph, we will discuss the present approach for jet noise calculation.

3.1.3 Thrust Calculation In accordance with traditional thrust definition, introduce P and the corresponding nondimensional value T as:

$$P = \int_{\Sigma_e} (\rho_e {u_e}^2 + p_e) d\Sigma - p_\infty \Sigma_e, \quad T = \frac{P}{p_o \Sigma_*} \tag{3.8}$$

where subscript indices e, ∞, o and $*$ are assigned to the nozzle exit cross section, ambient, total and critical (in the throat) parameters. Σ_* is the throat area. The integration is in some cross section downstream of the nozzle exit (or centerbody). The integrand in (3.8) is called an impulse function. Such a definition is introduced for rocket motors, but it does not take into account vehicle drag, and assumes the same shape of the external and internal vehicle surfaces. Therefore it only approximates the real vehicle net thrust. Nevertheless we will use this definition for an estimation of the nozzle shape variation influence on the thrust.

We can also define the thrust T directly by integration of the impulse function at the inlet cross section I_o, and the difference between pressure and friction along the nozzle wall. The integral of the impulse function at the nozzle exit, taking into account the boundary layer, allows us to estimate the integral error of the applied numerical scheme. Thus the thrust for a single design is calculated using the above nondimensional variables as:

$$T = B(I_o + I_1) - \frac{p_\infty}{p_o} \cdot \frac{\Sigma_e}{\Sigma_*}, \quad B = \frac{k}{\pi} \left(\frac{2}{\kappa + 1}\right)^{\frac{\kappa}{\kappa - 1}} \tag{3.9}$$

where

$$I_o = \int_0^{x(\varphi)} \int_{r_o}^{r_e} \int_0^{2\pi} p\left(1 - \frac{k}{2} {M_w}^2 c_f \sin\alpha\right) r dx dr d\varphi \tag{3.10}$$

$$I_1 = I(x_o) = \int_0^{r_o} \int_0^{2\pi} (p + \rho u^2) r dr d\varphi \tag{3.11}$$

where κ is the specific heat ratio, c_f is the friction coefficient, M_w is the local Mach number at the wall, u is velocity component in the direction of the nozzle-jet axis, α is the angle between this axis and the local tangent to the wall contour. The correction for calculation of thrust losses by the friction effect in the integral (3.10) is taken into account only for the cases of numerical simulation of mean flow in the inviscid approximation based on the Euler equations. When the numerical simulation of the mean flow is based on the full Navier-Stokes equations, this term in the integral must be substituted by the appropriate shear stress component at the wall, τ_x.

The calculation of the thrust for all cases of nozzles with impermeable and permeable shells based on formulae (3.8) have produced the following conclusions:

a) A jet flow exhausting from a convergent-divergent nozzle designed for exit Mach number, $M_e = 2.0$ with permeable and impermeable shells produces thrust which depends on the permeability coefficient K_p insignificantly for fixed nozzle pressure ratio, NPR, in the intervals NPR=6.31-9.47 and permeability K_p=0-0.2 considered. For example, for the overexpanded jet with NPR=6.31, the thrust equals T=0.489, and the deviation from this value with a variation of permeability changes the thrust within the limit of numerical simulation accuracy for the given grid. But the trust change can be significant with increase of nozzle pressure ratio. For an underexpanded jet with NPR=9.47 and K_p=0.1, the thrust is equal to 0.456, and for NPR=7.82 (free shock conditions) and K_p=0.1, the thrust is equal to 0.454. At the same time, the influence of the permeability on the shock wave structure is significant (see Figure 10), especially, in the jet.

b) Similar results were observed for a round nozzle with an axisymmetric centerbody with permeable and impermeable shells in the same interval of nozzle pressure ratio and permeability. Numerical simulations were conducted in the previous work [9] for the nozzle shown in Figure 4.a. For this case, the design Mach number at the nozzle exit equals M_e=3.67, i.e. the design nozzle pressure ratio is a free shock condition, NPR=96.34. Thus, the jets tested are overexpanded with the formation of reflected shock waves inside the nozzle and shell. The thrust for the nozzle with permeable and impermeable shells varies around the value, T=0.420, and also insignificantly depends on the permeability coefficient.

3.2 Jet Noise Calculation Methods and Acoustic Results

3.2.1 Jet Noise Calculation Methods.

It is well known ([14]) that turbulent mixing noise (TMN) is one of the main components of supersonic jet noise in addition to broadband shock noise (BSN) and screech tones (ST). In spite of this TMN contribution, in a common nozzle, the nearer jet exhaust conditions come to rated conditions, i.e. when the internal jet barrel shock system becomes weaker, the lower the noise level produced. The TMN source is turbulent small scale pulsations as well as large scale pulsations in the jet. With nozzle exit Mach number increase, the relative contribution of large scale turbulent pulsations to the TMN increases. This phenomenon is due to the fact that at nearsonic and supersonic phase speeds, sound radiation by these perturbations takes place by the mechanism of Mach wave radiation which is very effective. Thus, for the case of near perfectly expanded high-speed jets, prediction of the jet noise comes down to description of the large-scale turbulent evolution and evaluation of the sound generated by this turbulence. For axisymmetrical jets, a method based on this idea has been developed earlier (Tam & Morris 1980, Tam & Burton 1984, Tam & Chen 1994). Comparisons of the results obtained with the use of this method with the experimental data (Troutt & McLaughlin 1982, Seiner at al. 1982) and the results based on direct numerical simulation (Mitchell, Lele & Moin 1997, Mankbadi et al. 1998) shows favorable agreement.

The main assumptions underlying the method are the following:

1. Large-scale turbulence is described as a stochastic sum of spatially unstable disturbances of the jet (the so-called instability waves). Instability waves are the disturbances growing in the initial part of the jet owing to Kelvin-Helmholtz instability and decreasing at downstream parts of the jet where the shear layer becomes thick. The following steps are required to obtain the form of the instability waves. **a)** The mean flow in the jet is obtained from experimental data or numerical simulation of averaged turbulent Navier-Stokes equations. **b)** The non-stationary disturbances (instability waves) are obtained on the basis of the solution

of linearized Euler equations. The asymptotic method of expansion in small parameter and numerical simulation are used. The small parameter is provided by the large disparity in the spatial rate of change of the mean flow inside the jet in the radial and axial directions. In the first approximation, the spectral equations are solved to obtain the most unstable eigen-oscillations in the different cross-sections of the jet. In the second approximation, the amplitude equation is solved to relate the spectral equation solutions obtained in the first approximation for different cross-sections of the jet. **2.** Using the method of matched asymptotic expansions, the sound radiation generated by separate instability waves is obtained. **3.** The total turbulent mixing noise of the jet is obtained as a stochastic sum of the components generated by separate instability waves.

At present time, we have developed codes based on Tam's method which can be used for predicting the turbulent mixing noise for the case of an axisymmetrical supersonic jet. The next step in this direction is a generalization of Tam's method has be developed for the case of jets with cross-section of arbitrary form. Such generalization is aimed at jet noise reduction by means of nozzle geometry. It is possible that this factor may not have significant control over the noise generated by fine-grade turbulence (Tam, 1998, [16]). The point is that most of the fine-grade turbulence is generated in the region near the end of the jet potential core where the jet becomes near axisymmetrical independent of nozzle geometry. At the same time, the generation of the fine-grade turbulence is an essentially non-linear process and the maximum turbulence level is independent of the disturbance evolution in the upstream regions. On the contrary, these reasons do not control the large-scale turbulence. This is because the level of large-scale turbulence is determined by the increment of Kelvin-Helmholtz instability in the initial part of the jet. Hence, the noise generated by the large-scale turbulence should be dependent on the geometry of the nozzle.

3.2.2 Acoustics Calculation Results. Consider the influence of mean flow variation caused by the use of a permeable shell on the level of the noise generated by the jet. As was described above, the supersonic jet noise consists of three main components: turbulent mixing noise (TMN), broadband shock noise (BSN) and discrete tones (DT). The components BSN and DT are caused by the interaction of non-stationary disturbances and the barrel-shaped shock waves in the jet exhausting at off-design conditions. Therefore the level of BSN and DT must be decreased together with the intensity of the barrel-shock structures when the permeable shell is used.

The permeable shells also must be useful from the standpoint of decreasing of TMN. Indeed, for high-speed jets, the main source of the TMN in the direction of maximal radiation (30-40 degrees to the jet axis for M_e=2) is the large-scale turbulence. In this case, the generation mechanism of the TMN is Mach wave radiation by instability waves. An increase of instability waves is determined by the value of excitement of Kelvin-Helmholtz instability. This value has a maximum at the initial part of the jet, where the shear layer is very thin. It has been noted above that an injection of air through the wall of the permeable shell is the cause of a slowing down of the layers close to the shell wall. In other words, in this case the jet has a relatively thick mixing layer, Δr_m, at the exit of the shell (by comparison with the exit radius, r_e, namely, $\Delta r_m/r_e$ =0.15). That must diminish the value of the instability excitement in the initial part of the jet, and, correspondingly, must decrease the TMN level. To an even greater degree, this conclusion relates to the higher harmonics and high-frequency part of the spectrum where the disturbances have wavelength comparable with the initial thickness of the mixing layer.

This qualitative conclusion is confirmed by the results of numerical calculation of the TMN. Some of these results are presented in Figure 12. The method permits to obtain the results within the accuracy of one arbitrary additive constant (in dB scale). This constant is chosen to fit the known experimental data on the supersonic jet noise (Seiner, McLaughlin, Liu 1982 [17]). The near sound field for case II is shown in Figures 12a,b. The TMN levels obtained are characteristic of the direction of maximum radiation which is approximately at the angle of 30 degrees to the jet axis. The comparison of the TMN far field levels for the cases I (dashed lines) and II (solid lines) at the angle of 30 degrees is presented on Figures 12c-e. One can see that an increase of the initial value of the mixing layer thickness (from 0.05 to 0.15) causes a diminishing of the TMN, especially for the frequencies St>0.2-0.3 and for harmonics

n=1 and n=2.

IV. CONCLUSION

Several experimental acoustic tests were conducted in the anechoic chamber AK-2 at the Central Aerohydrodynamics Institute (TsAGI, Moscow) in Russia. These tests examined the influence of permeable shells on the noise from a supersonic jet exhausting from a round nozzle designed for exit Mach number, M_e=2.0, with conical and Screwdriver-shaped centerbodies. Significant acoustic benefits of permeable shell applications were obtained for overexpanded jets by comparison with impermeable shell applications. The noise reduction in the overal pressure level was obtained up to ~5-8%. Numerical simulations of a jet flow exhausting from a convergent-divergent nozzle designed for exit Mach number, M_e=2.0, with permeable and impermeable shells were conducted at the NASA LaRC and Hampton University. Two numerical codes were used. The first was the NASA LaRC CFL3D code for accurate calculation of jet mean flow parameters on the basis of a full Navier-Stokes solver (NSE). The second was a numerical code based on Tam's method for turbulent mixing noise (TMN) calculation. The thrust calculations for this problem have shown in some cases insignificant thrust loss due to permeable shell application and, for overexpanded jets, even some thrust augmentation. Numerical and experimental results are in good qualitative agreement.

V. ACKNOWLEDGEMENTS

We would like to acknowledge the NASA LaRC Jet Noise Team's support and help, Drs. Dennis Bushnell, John M. Seiner, and Jay C. Hardin for their attention, interest to our research, reviews and useful suggestions. This research was conducted under the CRDF grant, #RE-136, which is the support for several other projects conducted under the NASA grants, ##NAG-1-1835, 1936, and #2249.

VI. REFERENCES

1. Transonic Testing Techniques (A Simposium), 1954, IAS S.M.F. Fund Paper No. FF-12, Edited by H.L. Dryden, National Summer Meeting, June 21-24, 1954, Los Angeles, CA.

2. Grodzovsky, G.L., Nikolsky, A.A., Svischev, G.P., and Taganov, G.I., 1967, Supersonic Gas Flows into Perforated Boundaries, Mashinostroenie, Moscow, 1967, 144p.

3. Rukhmatulin, Kh.A., Flow around permeable body, 1950, Vestnik of Moscow State University, Phys.-Math. and Natural Series, (in Russian), 1950, No.3.

4. Maestrello, L., Apparatus and Method for Jet Noise Suppression, 1983, US Patent #4,398,667.

5. Maestrello, L., An Experimental Study on Porous Plug Jet Noise Suppressor, 1979, AIAA Paper #79-0673, 5th AIAA Aeroacoustics Conference, March 12-14, 1979, Seattle, WA.

6. Flax, A.H., et al., Development and Operation of the C.A.L. Perforated-Throat Transonic Wind Tunnel, 1954, IAS S.M.F. Fund Paper No. FF-12, pp.1-41.

7. Cornell W.G., 1958, Losses in Flow Normal to Plane Screens, Trans. ASME, May, 1958, pp.791-799.

8. Guvernuk, S.V., and Ulyanov G.S., 1975, Supersonic Flow at the plate with perforated tail portion, Proceeding of Institute of Mechanics, Moscow State University (in Russian), 1975, pp.96-104.

9. Gilinsky, M.M., Kouznetsov, V.M., and Nark, D.M., 1998, Acoustics and Aeroperformance of Nozzles with Screwdriver-Shaped and Axisymmetric Plugs, AIAA Paper #98-2261, 4th AIAA/CEAS Aeroacoustics Conference, June 2-4, 1998, Toulouse, France.

10. Krist, S.L., Biedron, R.T., and Rumsey, C.L., 1996, CFL3D User's Manual (Version 5.0), NASA Langley Research Center, 311p.

11. Molvik, G.A. and Merkle, C.L. 1989, A Set of Strongly Coupled, Upwind Algorithms for Computing Flows in Chemical Nonequilibrium, AIAA Paper 89-0199, 27th Aerospace Sciences Meeting, Jan. 9-12.

12. Godunov, S.K. et al., 1976, Numerical Solution of Multidimensional Problems of Gas Dynamics, Moscow: Nauka, 1976, 400p.

13. Menter, F. "Improved Two-Equation $k-\omega$ Turbulence Models for Aerodynamic Flows,"NASA TM 103975, 1992.

14. Tam C.K.W. Supersonic jet noise. 1995, Annual Review of Fluid Mechanics, V. 27, 1995, pp.17-43.

15. Tam C.K.W., Morris P.J. The radiation of sound by the instability waves of a compressible plane turbulent shear layer. J. Fluid Mech.,V.98, 1980, pp. 349-381.

16. Tam C.K.W. Influence of nozzle geometry on the noise of high-speed jet. AIAA J., V.36, 1998, pp.1396-1400.

17. Seiner J.,M., McLaughlin D.,K., Liu C.,H. 1982, Supersonic jet noise generated by large-scale instabilities, NASA Technical Paper 2072, 42p.

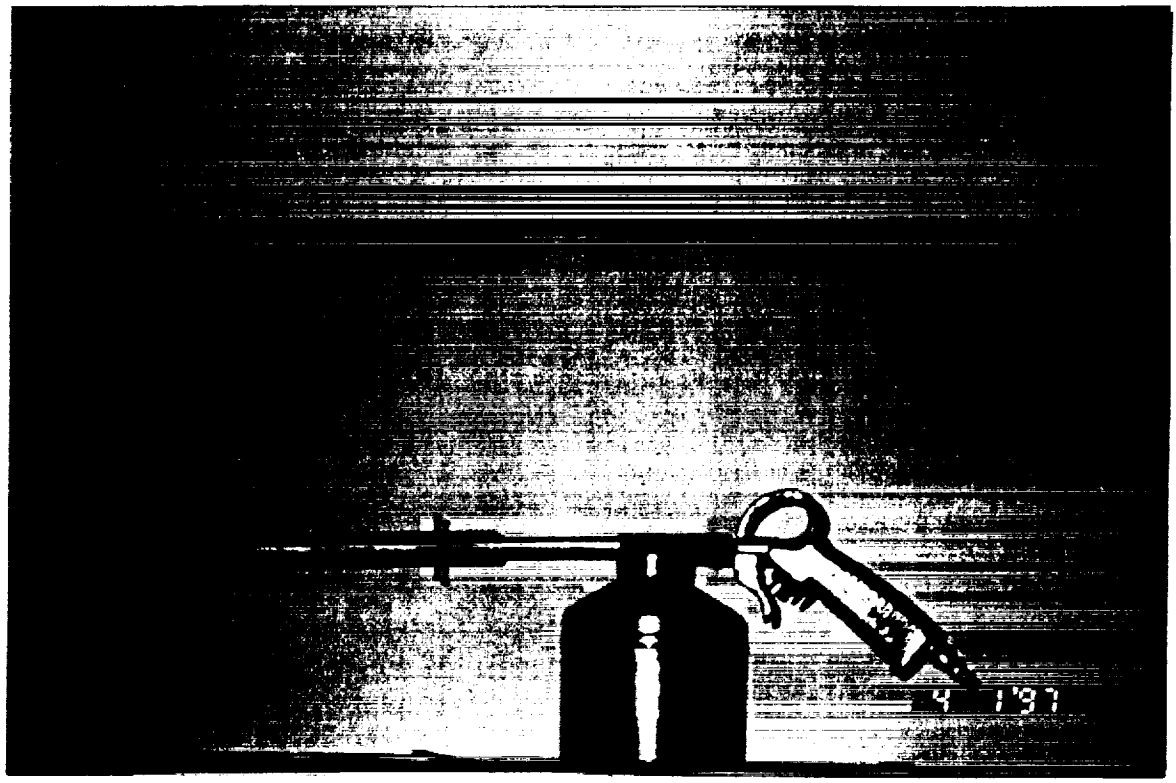

a)

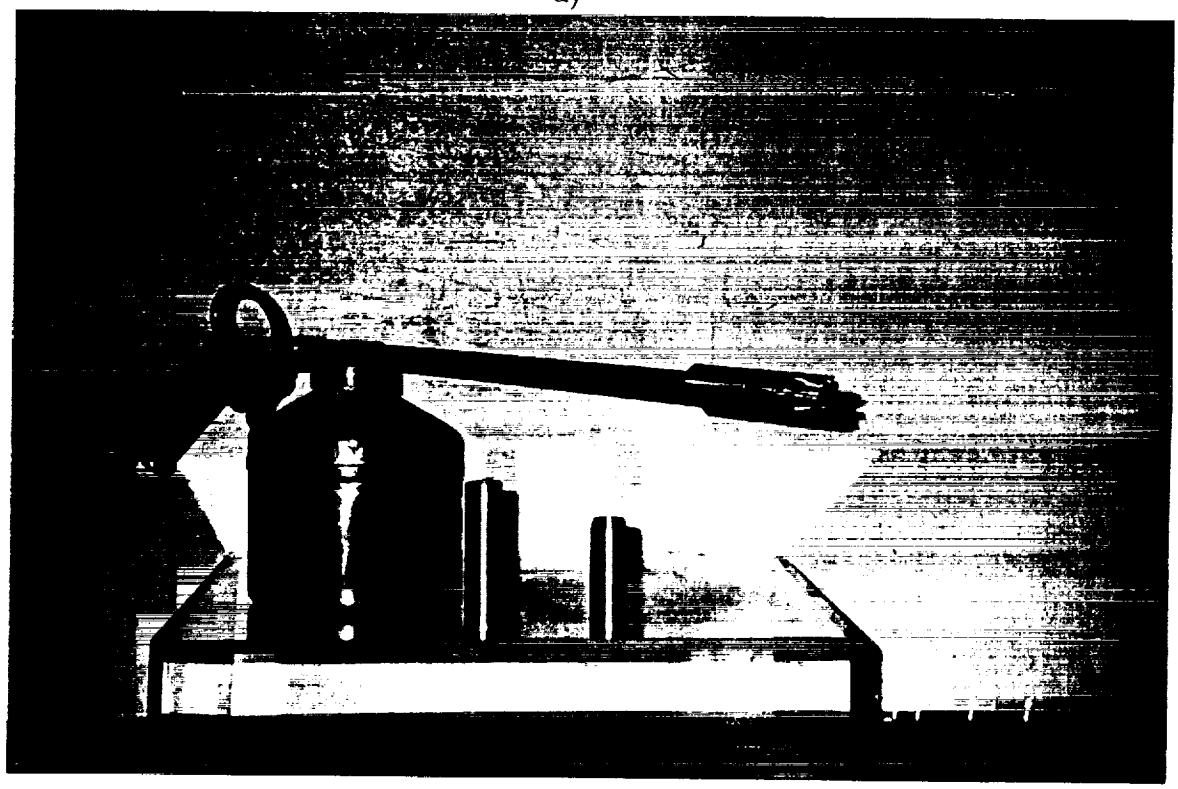

b)

Fig.1 Two spraying devices with permeable and impermeable shells tested at the NASA LaRC. **a)** the shell is the long small tickness pipe; **b)** the shell is the short large tickness pipe.

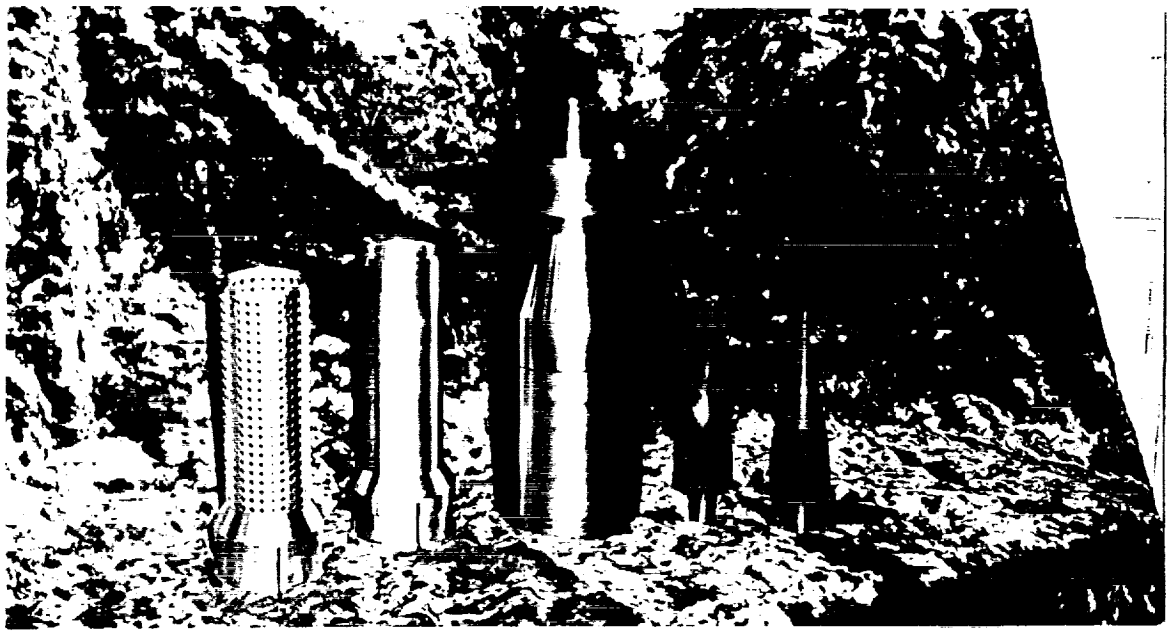

Fig.2 The convergent-divergent (CD) conical nozzle (center), **Screwdriver** and **Conical** centerbodies (right), and solid and perforated shells (left) which were tested in the anechoic chamber AK-2 at the TsAGI, Moscow.

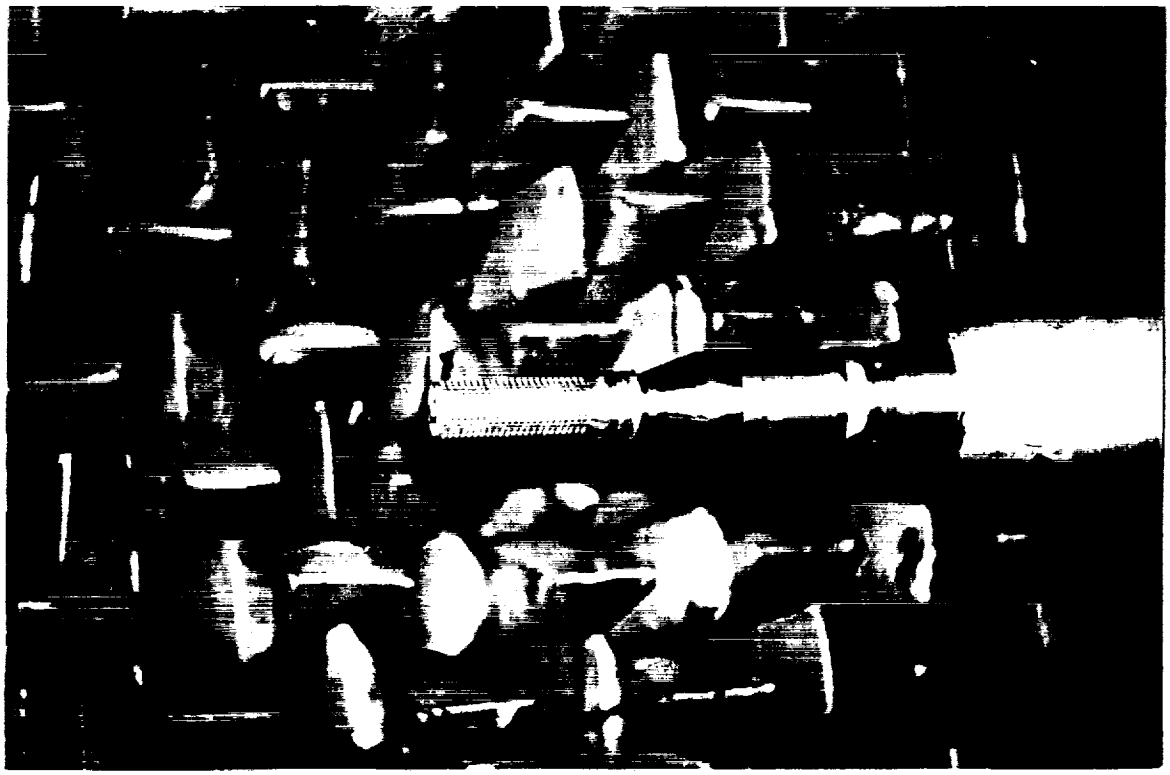

Fig.3 Existing CD conical nozzle with the **Screwdriver** centerbody and perforated shell mounted in the AK-2 (TsAGI, Moscow).

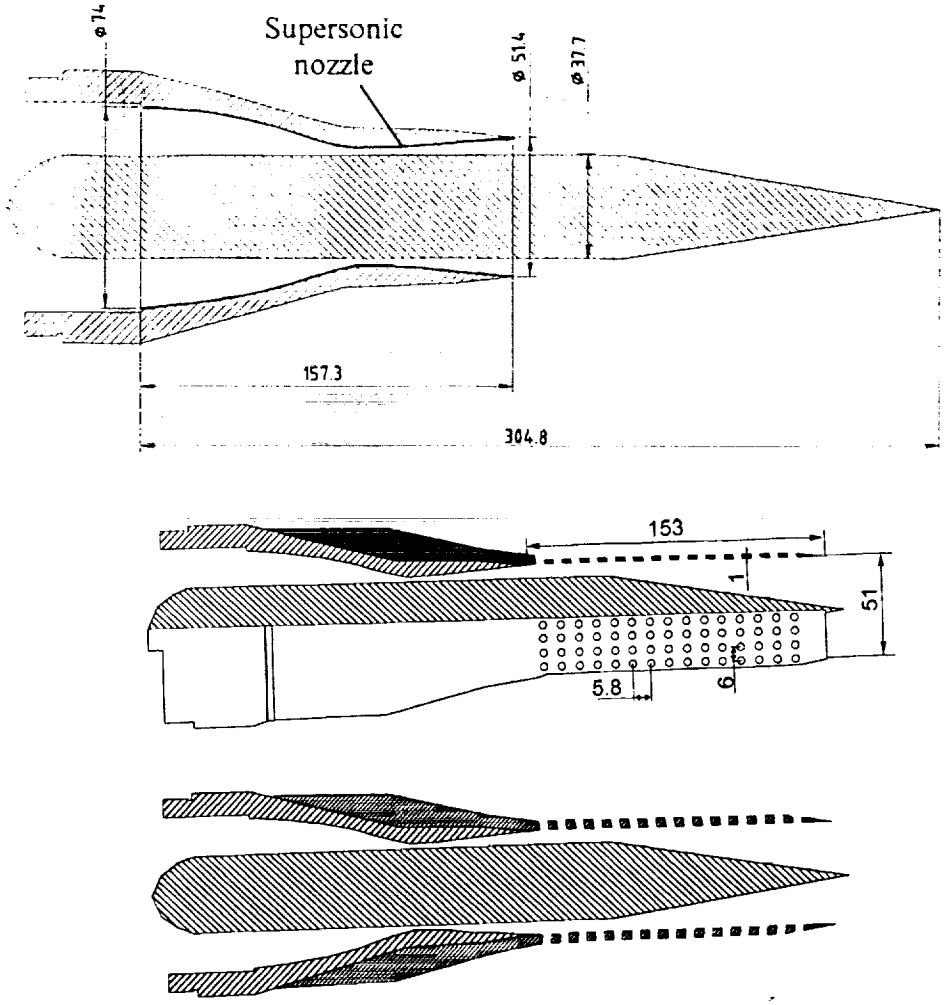

Fig.4 The picture of the nozzle with the conical centerbody without the shell (a) and with the perforated shell (b). The main sizes are in millimeters (mm.).

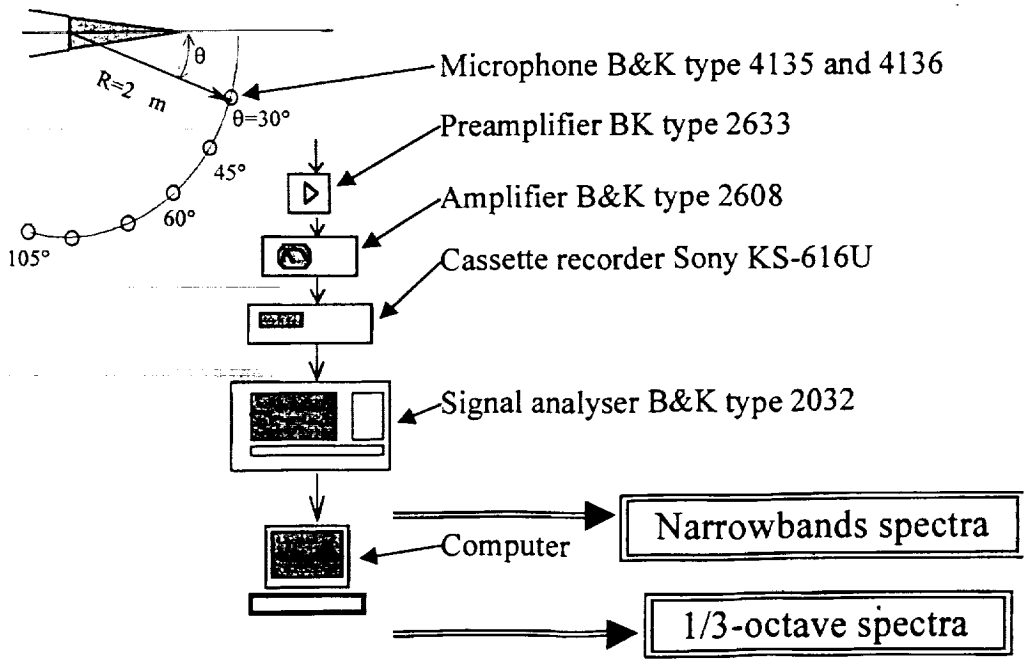

Fig.5 The scheme measurement in the anechoic chamber AK-2 at the TsAGI, Moscow, and the scheme of automatic data processing.

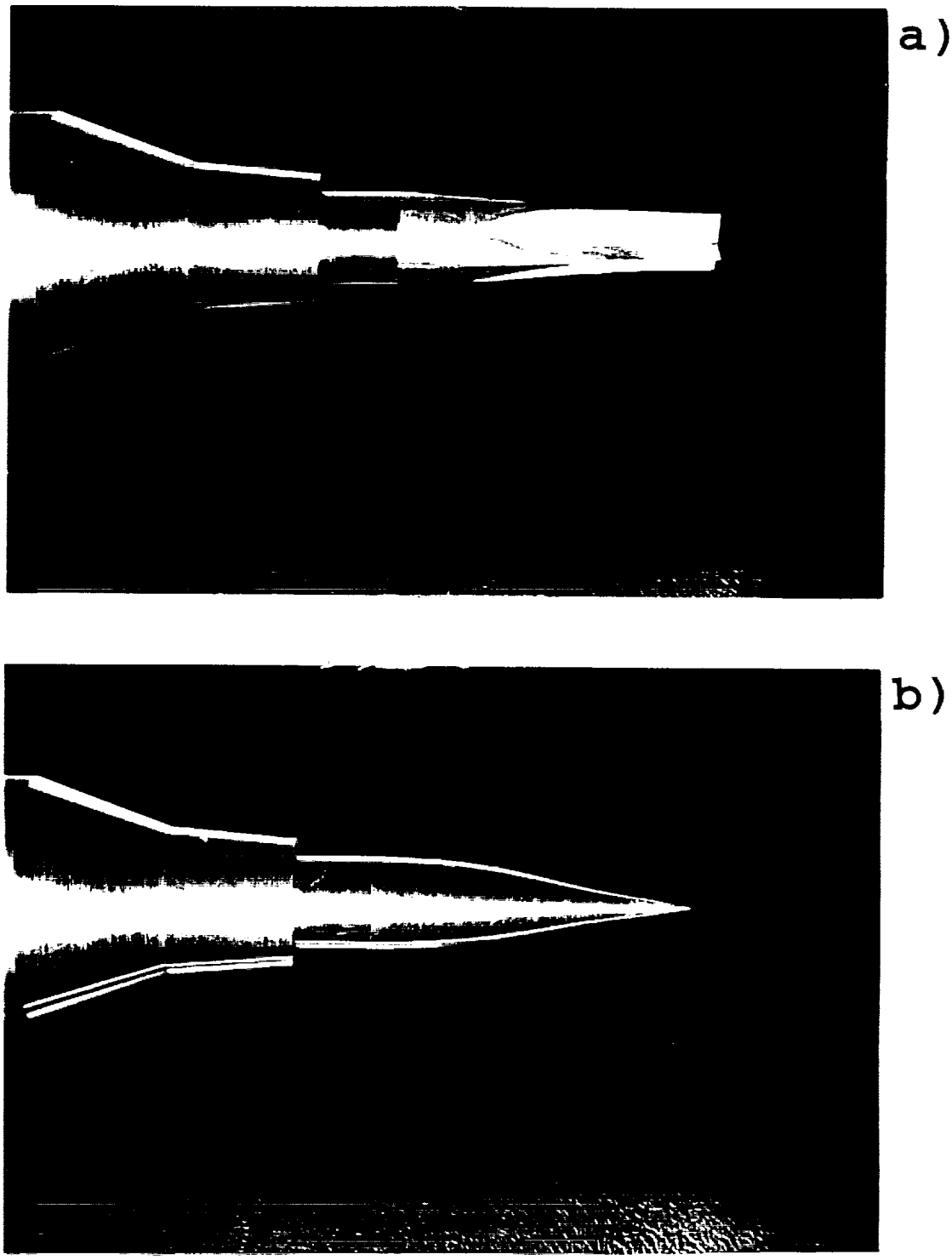

Fig.6 Axisymmetric convergent-divergent nozzle with the Screwdriver-shaped (a) and axisymmetric (b) centerbodies. Both centerbodies have the same areas at the cross section located on the same distance, $x = x_i$=const, from the throat, $x = 0$. These designs were tested in the anechoic chamber at the TsAGI, Moscow.

Case No.	NPR	Nozzle Configuration
1	4.5	CCB without Shell
2	4.5	CCB with Perforated Shell
3	4.5	CCB with Solid Shell
4	4.5	SdCB without Shell
5	4.5	SdCB with Perforated Shell
6	4.5	SdCB with Solid Shell
7	4.5	CCB without Shell
8	3.5	CCB without Shell
9	2.5	CCB without Shell
10	2.5	CCB with Perforated Shell
11	2.5	CCB with Solid Shell
12	2.5	SdCB without Shell
13	2.5	SdCB with Perforated Shell
14	2.5	SdCB with Solid Shell

Table 1. Acoustic tests at the TsAGI
Abbriviations: CCB-Conical Centerbody, SdCB-Screwdriver Cenerbody.

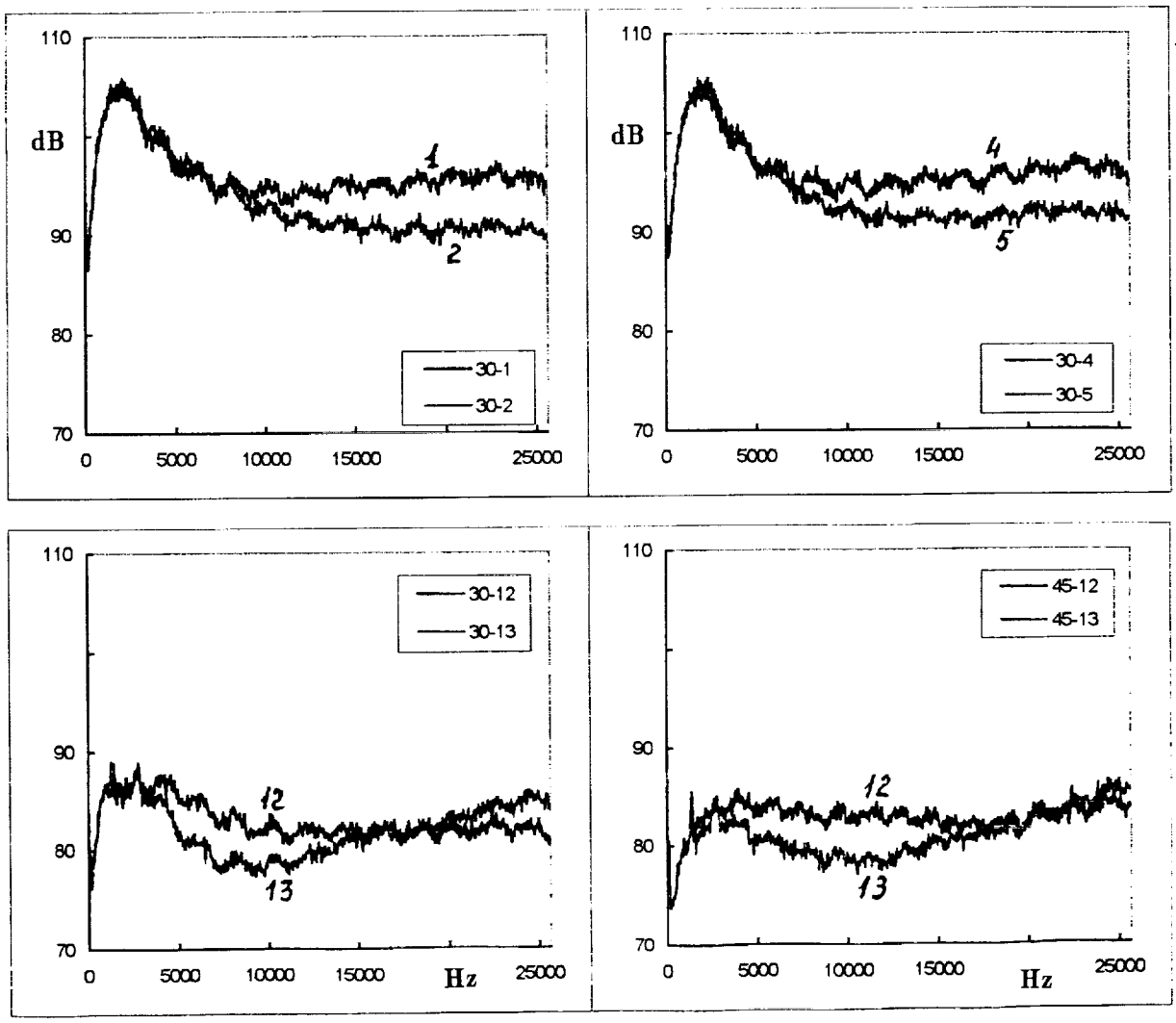

Fig.7a-d. The acoustic power spectral density vs frequency for two observation angles; two cases comparison in each figure.

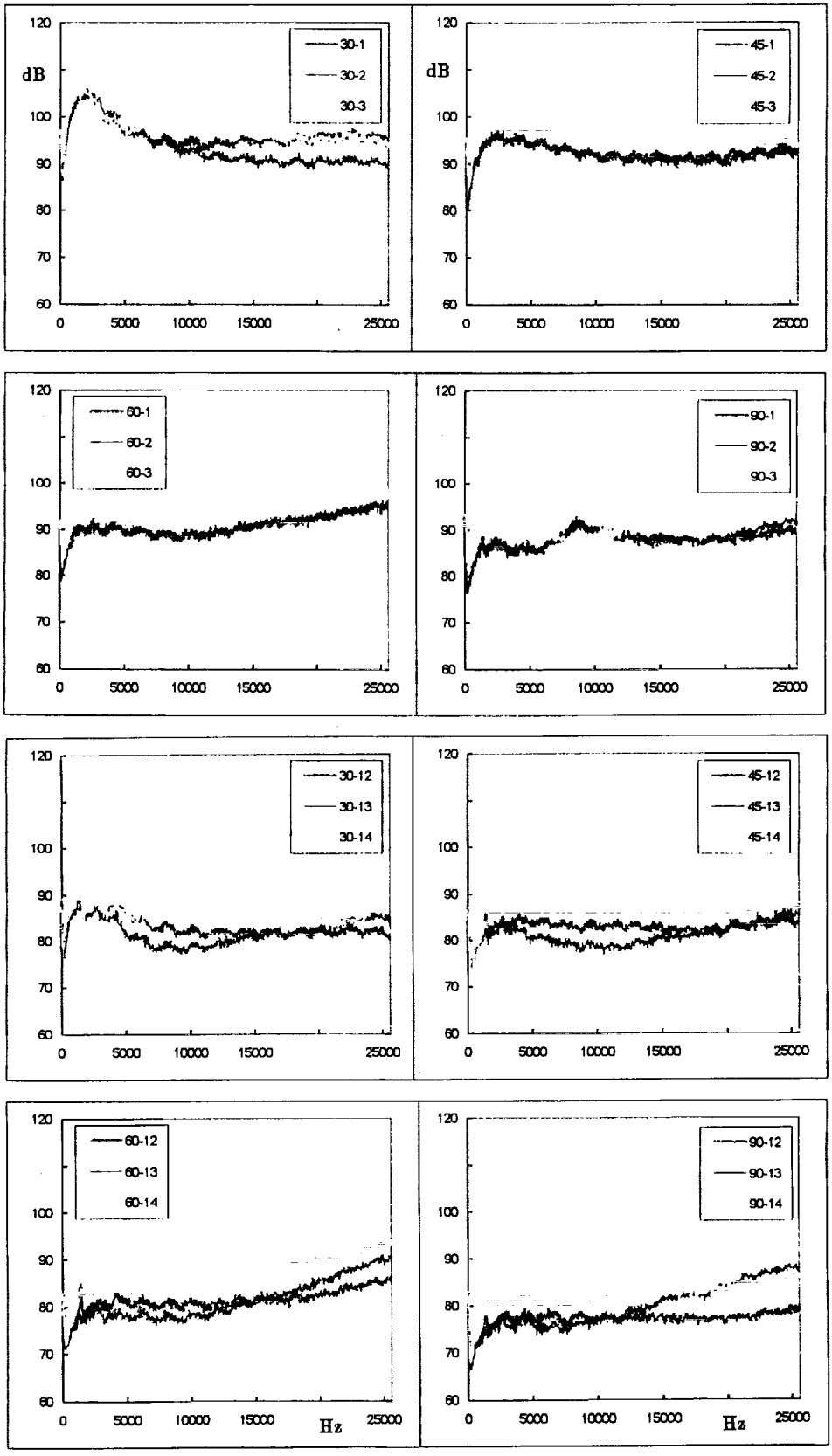

Fig.8 Narrowband spectra density vs frequency for different cases shown in Table 1.

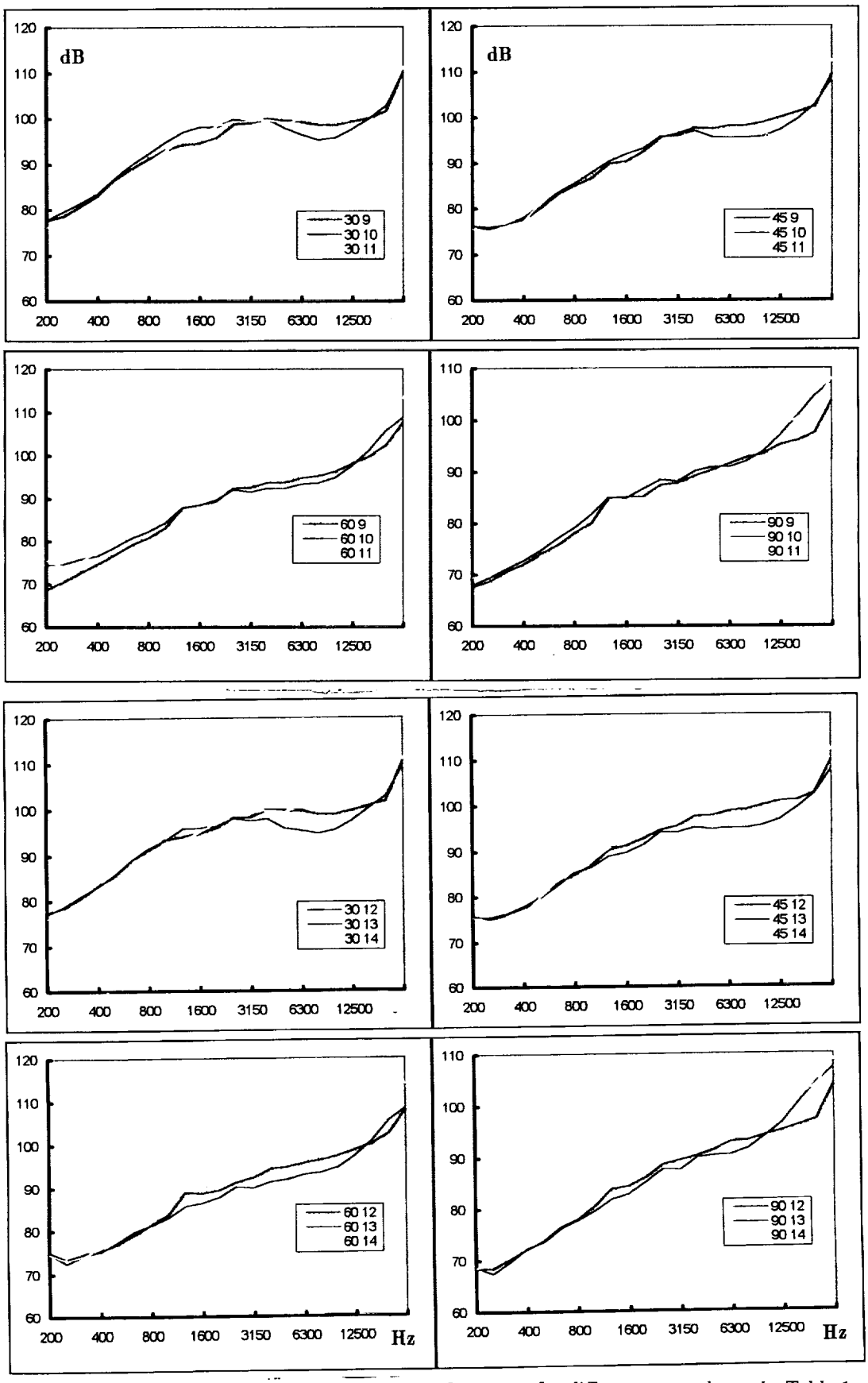

Fig.9 1/3-octave band spectra density vs frequency for different cases shown in Table 1.

NOZZLE WITH IMPERMEABLE AND PERMEABLE SHELLS

MACH CONTOURS

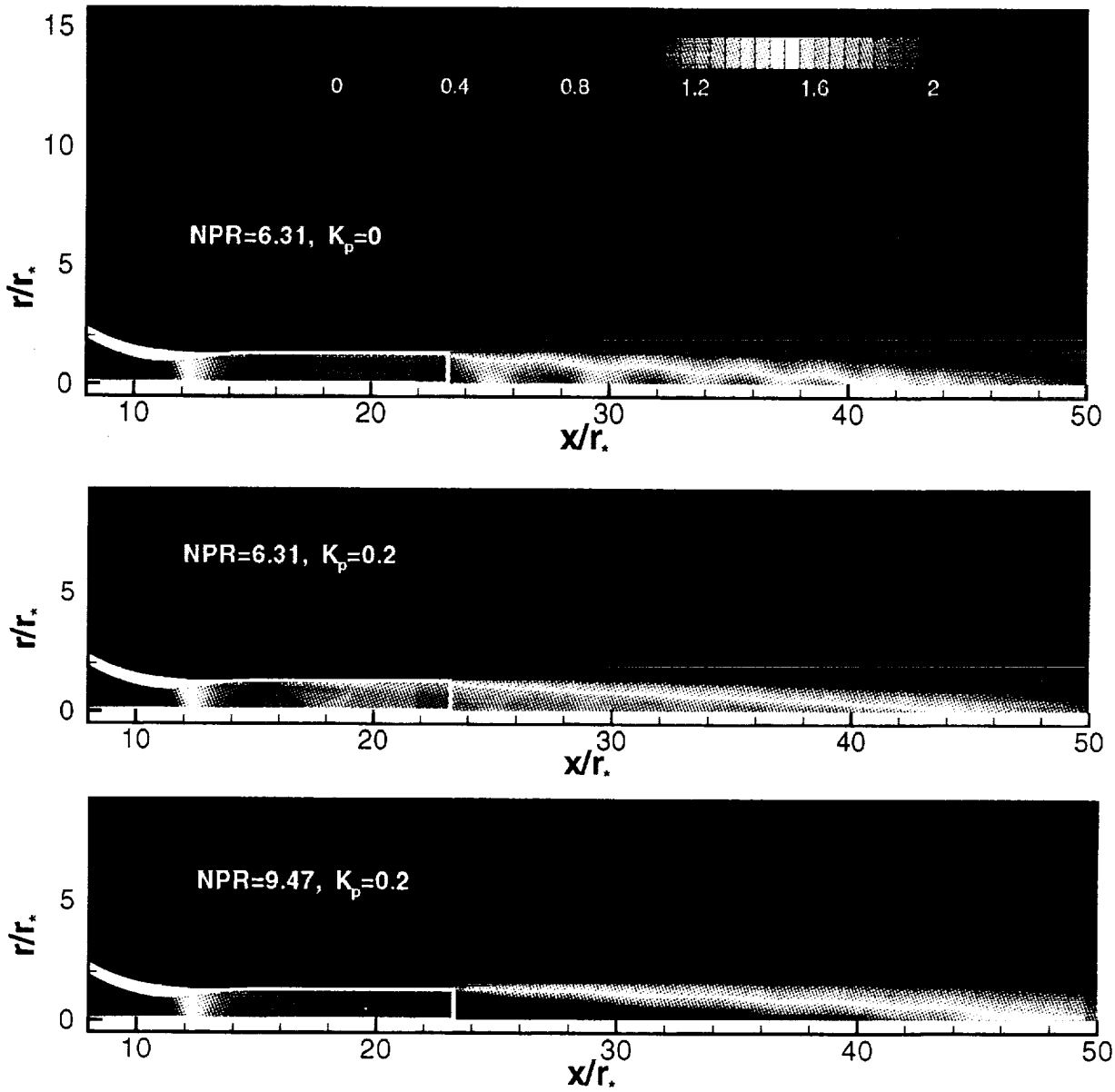

Fig.10 Mach contours for the supersonic flows inside the CD nozzle designed for the exit Mach number, M_e=2.0, and in the exhausting jets for three cases: **a)** the upper picture-impermeable shell (permeability coefficient, K_p=0), overexpanded jet with the nozzle pressure ratio, NPR=6.31; **b)** the middle picture-permeable shell with K_p=0.2 and NPR=6.31; **c)** the lower picture-permeable shell with K_p=0.2, underexpanded jet with NPR=9.47.

NOZZLE WITH IMPERMEABLE AND PERMEABLE SHELLS

PRESSURE CONTOURS

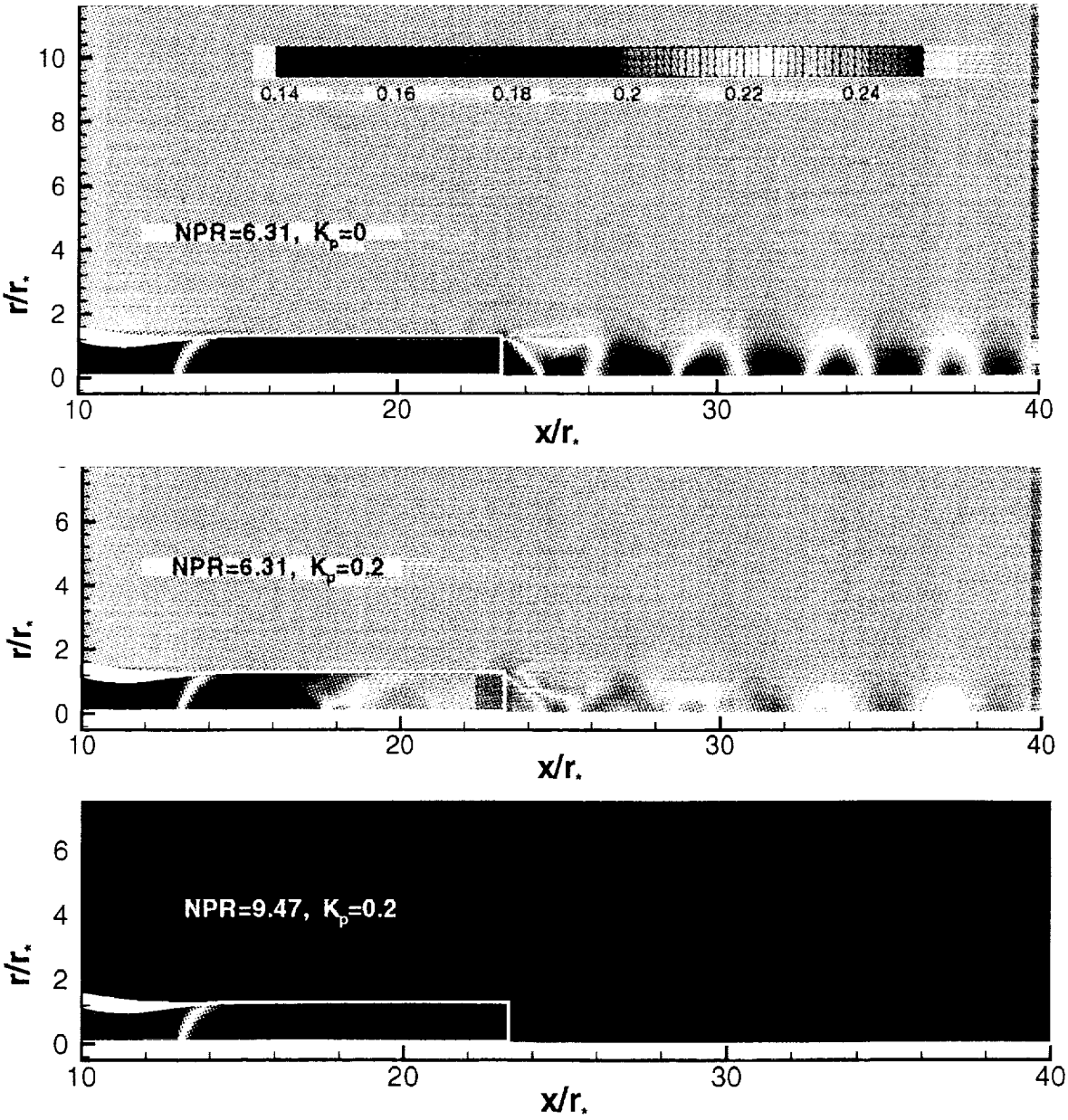

Fig.11 Pressure contours for the supersonic flows inside the CD nozzle designed for the exit Mach number, M_e=2.0, and in the exhausting jets for three cases: **a)** the upper picture-impermeable shell (K_p=0), overexpanded jet with the nozzle pressure ratio, NPR=6.31; **b)** the middle picture-permeable shell with K_p=0.2 and NPR=6.31; **c)** the lower picture-permeable shell with K_p=0.2, underexpanded jet with NPR=9.47.

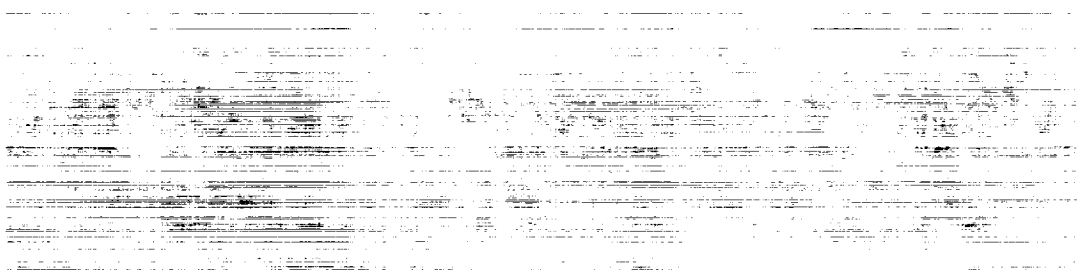

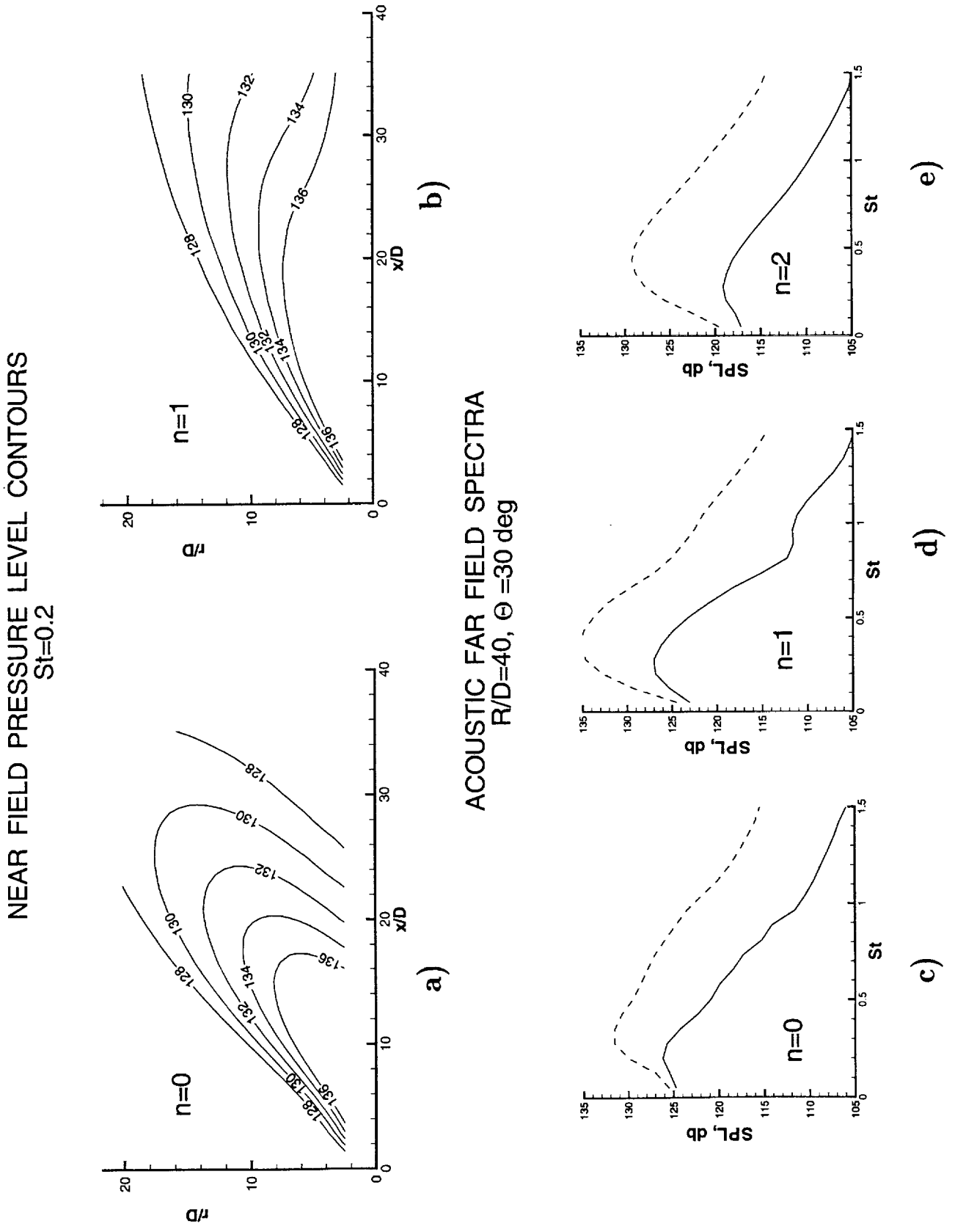

Fig.12 Near anf far field spectra for the first three harmonics, n=0,1, and 2.